DOI:
10.1016/j.jid.2016.03.041

Document Version
Peer reviewed version

Accepted Manuscript

A powerful mitochondria-targeted iron chelator affords high photoprotection against solar ultraviolet A radiation

Olivier Reelfs, Vincenzo Abbate, Robert C. Hider, Charareh Pourzand

PII: S0022-202X(16)31053-3

DOI: 10.1016/j.jid.2016.03.041

Reference: JID 298

To appear in: *The Journal of Investigative Dermatology*

Received Date: 14 December 2015

Revised Date: 8 March 2016

Accepted Date: 12 March 2016

Please cite this article as: Reelfs O, Abbate V, Hider RC, Pourzand C, A powerful mitochondria-targeted iron chelator affords high photoprotection against solar ultraviolet A radiation, *The Journal of Investigative Dermatology* (2016), doi: 10.1016/j.jid.2016.03.041.

A powerful mitochondria-targeted iron chelator affords high photoprotection against solar ultraviolet A radiation

Olivier Reelfs[1]*, Vincenzo Abbate[2]*, Robert C. Hider[2] and Charareh Pourzand[1**]

[1] Department of Pharmacy and Pharmacology, University of Bath, Claverton Down, Bath BA2 7AY, United Kingdom.
[2] Institute of Pharmaceutical Science, King's College London, Franklin-Wilkins Building, 150 Stamford Street, London SE1 9NH, United Kingdom.

* These authors contributed equally.

**Corresponding author: Charareh Pourzand, Department of Pharmacy and Pharmacology, University of Bath, Claverton Down, Bath BA2 7AY, United Kingdom. Email: prscap@bath.ac.uk

Short title:
Photoprotective mitochondrial iron chelator

Abbreviations: Dns, dansyl; ER, endoplasmic reticulum; Hbl, Nε-2.3-dihydroxybenzoyllysine; LI, labile iron; LIP, labile iron pool; MW, molecular weight; ROS, reactive oxygen species; TMRM, tetramethylrhodamine methyl ester; UVA, ultraviolet A.

ABSTRACT

Mitochondria are the principal destination for labile iron (LI), making these organelles particularly susceptible to oxidative damage upon exposure to ultraviolet A (UVA**,** 320-400 nm), the oxidizing component of sunlight. The LI-mediated oxidative damage caused by UVA to mitochondria leads to necrotic cell death via ATP depletion. Therefore targeted removal of mitochondrial LI via highly specific tools from these organelles may be an effective approach to protect the skin cells against the harmful effects of UVA. In this work, we designed a mitochondria-targeted hexadentate (tricatechol-based) iron chelator linked to mitochondria-homing SS-like peptides. The photoprotective potential of this compound against UVA-induced oxidative damage and cell death was evaluated in cultured primary skin fibroblasts. Our results show that this compound provides unprecedented protection against UVA-induced mitochondrial damage, ATP depletion and the ensuing necrotic cell death in skin fibroblasts and this effect is fully related to its potent iron-chelating property in the organelle. This mitochondria-targeted iron chelator has therefore promising potential for skin photoprotection against the deleterious effects of UVA component of sunlight.

Key words: labile iron - iron chelator - mitochondria - oxidative stress - UVA - photoprotection – skin – fibroblasts - ROS

INTRODUCTION

The ultraviolet A (UVA, 320-400 nm) component of sunlight is weakly absorbed by most biomolecules but is predominantly oxidative in nature, generating reactive oxygen species (ROS) via photochemical interactions involving non-DNA cellular chromophores (Tyrrell, 1996). In addition, the presence of a cellular pool of iron bound to small ligands, called labile iron pool (LIP), sensitizes cells to UVA as it can catalyse the formation of toxic oxygen-containing radicals (Hider and Kong, 2013; Cabantchik, 2014) such as hydroxyl radical ($^{\bullet}OH$) via Fenton chemistry (Winterbourn, 2008). This can ultimately overwhelm the cellular antioxidant defense mechanisms and lead to cell damage and death (Reelfs et al., 2004; Reelfs et al., 2010; Ma et al., 2015).

Originally, LIP was considered to be cytosolic, however recent studies have indicated that only a small proportion of the intracellular redox-active pool of LI resides in the cytosol (Aroun et al., 2012; Ma et al., 2015). Indeed due to constant need for LI in various cellular functions, cytosolic LIP is usually rapidly relocated to distinct subcellular compartments, notably lysosomes and mitochondria, which are the dominant sites for iron redistribution as well as iron sequestration and incorporation into proteins (Reelfs et al., 2010; Sohn et al., 2008; Levi and Rovida, 2009; Fakih et al., 2008). Mitochondria require a continuous provision of LI from the cytosol as they are the main site for heme and iron–sulfur cluster synthesis which are then exported to other cell compartments (Hider and Kong, 2013). Several mechanisms appear to account for mitochondrial iron uptake. In addition, mitoferrins 1 and 2 have been involved in iron transport to mitochondria in a range of organisms (Paradkar et al., 2009; Shaw et al., 2006). As a result of iron influx, the concentration of LI in the mitochondrial matrix exceeds significantly that of cytosol (Petrat et al., 2001; Petrat et al., 2002), which make these organelles highly susceptible to oxidative damage. Consequently, since mitochondria are the major sites of oxygen consumption and LI is also a strong catalyst of harmful ROS formation, the simultaneous

presence of oxygen and iron appears to be detrimental to the organelles (Levi and Rovida, 2009). Excessive mitochondria-mediated ROS production can promote oxidative damage to mitochondrial components, impeding key mitochondrial functions, notably ATP synthesis, heme synthesis and iron sulfur cluster assembly (Murphy, 2009; Aroun et al., 2012). Oxidative damage to mitochondria will also permeabilize mitochondrial outer membrane resulting in the leakage to the cytosol of cytochrome c (cyt c). This will activate the cell's apoptotic or necrotic pathway, depending on the extent of the oxidizing insult (Pourzand and Tyrrell, 1999; Shidoji et al., 1999). In the event of severe oxidative damage to mitochondrial membranes, ATP depletion will lead to cell death via necrosis because apoptosis involves energy-requiring steps, especially in the formation of the apoptosome complex between apoptosis protease activating factor -1 (Apaf-1) and cyt c *(*Zou et al*.,* 1999; Leist et al., 1997; Li et al., 1997; Green and Reed, 1998).

Mitochondria are endowed with protective mechanisms against iron-catalyzed ROS-induced damage. Nevertheless, these organelles remain highly sensitive to oxidative damage as deregulation in mitochondrial iron homeostasis has been linked to the development of pathological conditions and cell death (Levi and Rovida, 2009; Kakhlon et al., 2010). In this context, we have shown that UVA radiation or H_2O_2 treatment of human skin fibroblasts and Jurkat T leukemia cell line in culture leads to both immediate oxidative damage to mitochondrial membrane and a concomitant rise in the cytosolic LIP (Zhong et al., 2004; Yiakouvaki et al., 2006; Al-Qenaei et al., 2014). As a result of mitochondrial membrane damage, the electron chain reactions are disrupted leading to the excessive generation of ROS and mitochondrial ATP depletion that ultimately causes necrotic cell death. Additionally, it has been shown that both UVA and H_2O_2 induce oxidative damage to mitochondrial DNA, with potential implication in photoaging, and skin cancer (Berneburg et al., 1999; Krishnan and Birch-Machin, 2005; Oyewole et al., 2014).

Because mitochondria are a major source of ROS, much effort has been focussed on the design of mitochondria-targeted antioxidant compounds such as MitoQ, a ubiquinone derivative

conjugated to triphenylphosphonium that enables this molecule to enter the mitochondria (James et al., 2007). An unrelated compound, 4,5-dihydroxy-1,3-benzenedisulfonic (tiron), a catechol-based metal sequestering agent with ROS scavenging properties, has been described as being able to permeabilize the mitochondrial membrane and thereby be localized in the mitochondrion from the cytoplasm (Krishna et al., 1992; McArdle et al., 2005; Tulah and Birch-Machin, 2013). Such antioxidants have been shown to protect against UVA- and H_2O_2-induced mitochondrial DNA damage. Despite the attractive nature of these protective strategies, such 'conventional' antioxidants which scavenge mitochondrial ROS will have only a limited protective effect in the skin particularly at the level of mitochondria. This is because they cannot properly address the presence of excess LI in the organelle which is the major contributor to the generation of highly reactive ROS and oxidative damage especially upon exposure of cells to strong oxidising agents such as UVA (Reelfs et al., 2010).

The challenge of countering the effects of the combination of UVA and iron-catalysed excess ROS formation in the mitochondria highlights a clear need for the development of mitochondria-targeted iron chelating agents in order to adjust and remove the excess harmful pool of mitochondrial LI. Limited exposure of cultured fibroblasts and keratinocytes to the strong iron chelator desferrioxamine (DFO) protects skin cells against biologically relevant UVA doses. Nevertheless, despite being a strong iron chelator, DFO is not an adequate choice for use in skin photoprotection via topical application, due to its hydrophilicity and elevated molecular weight (MW) (Reelfs et al., 2010). Although bidentate iron chelators (*e.g.* catechols and hydroxypyridinones) possess adequate lipophilicity and MW, they have a weak iron scavenging ability at low iron concentrations. This is a major drawback in their use for skin photoprotection via topical application (Liu and Hider, 2002). We therefore decided to opt for hexadentate analogues as these compounds would have similar structures to siderophores (Hider and Zhou, 2005) and would have a high iron scavenging ability despite possessing elevated MW.

A powerful mitochondria-targeted hexadentate tricatechol-based iron chelator was synthesized and evaluated in cells in culture for its protective effects against UVA-induced iron-catalyzed oxidative damage and cell death. We demonstrate that this compound is capable of protecting mitochondria and thereby skin cells from the deleterious effects of UVA component of sunlight.

RESULTS

Compound design and synthesis

We have recently demonstrated the successful use of mitochondria-targeted 'SS-peptides' for the delivery of iron-specific sensors to the mitochondria (Abbate et al., 2015a and b). We therefore chose the same approach to target an iron chelator to the mitochondria.

The catechol-based hexadentate iron chelator described in this study possesses the following properties (i) high affinity for iron (pFe >25) and (ii) the iron-complexes do not redox cycle at physiological pH. These properties render compound **2** suitable for skin photoprotection.

Table S1 and Figure 1 document the structures of the compounds investigated in this study. Compound **1** is a simple SS-type mitochondria-targeted peptide which we designed to form the leading mitochondrial address signal to which we have linked an hexadentate chelator to form compound **2**. Compound **3** is a fluorescent version of compound **2** possessing a dansyl fluorophore (Dns) which renders it possible to follow its subcellular localization by fluorescence microscopy. We have previously shown that the Dns fluorophore (absorption and emission maxima: 330 and 546 nm, respectively) is a suitable choice as it does not alter the biological function of the chelator-peptide (Abbate et al., 2015a and b). Finally, in compound **4**, hemi-methylation of one of the catechol groups renders this compound less efficient at binding iron than its counterpart compound **2**. Table S2 provides some relevant physico-chemical properties of the compounds and Figure S1 their HPLC profiles. Although the $clogD_{7.4}$ value for compound **2** is low (-2.05, Table S2), it is 3 orders of magnitude larger than that of the parent peptide **1** (-

5.39). Peptide **1** is able to penetrate membranes with relative ease (Zhao et al., 2004) probably by the formation of lipid-peptide complexes. We anticipate that compound **2** will have similar properties especially as it is markedly less hydrophilic than peptide **1**.

Subcellular localisation of the chelator-peptide in human primary skin fibroblasts

Using fluorescence microscopy, we first investigated the subcellular localization of compound **3** in primary skin fibroblast FEK4 cells. Cells were incubated with compound **3** and co-stained with a fluorescent marker specific for mitochondria, lysosomes or endoplasmic reticulum (ER) as described in "Cell biology" section in Supplementary Information file. Colocalization of compound **3** to specific organelles was evaluated qualitatively by (i) the occurrence of composite fluorescent yellow signal generated by the co-occurrence of both green and red fluorescent signals above a threshold level (Figure 2) and (ii) intensity profile comparison (Figure S2). Quantitative evaluation of the extent of colocalization was performed as described in Supplementary Information file. The results of both qualitative and quantitative analyses revealed that compound **3** was able to penetrate cells and accumulate preferentially into mitochondria (Figure 2, panels a-d). This tropism for mitochondria was specific, as we could not observe any colocalization with lysosome/endosome (Figure 2, panels e-h) or ER compartments (Figure 2, panels i-l). The same subcellular pattern of localization was observed for compound **3** using FCP7 (primary skin fibroblasts from another donor) which we have previously studied in our laboratory (Zhong et al., 2004). Representative pictures and intensity profiles are presented in Figure S5a.

UVA-induced cell death is prevented by the tricatechol peptide

In order to highlight the photoprotective role of iron chelation strategy in exposure to solar UV, we chose to use a broad-spectrum UVA lamp (320-400nm) rather than the whole UV spectrum

as a light source. This has the notable advantage to allow to demonstrate the UVA-specificity of the biological effects observed.

To evaluate the photoprotective capability of compound **2** against UVA-induced cell death, we chose the UVA dose of 500 kJ/m^2 which is equivalent to 140 min uninterrupted sun exposure at sea level (Pourzand et al., 1999). This is a high but still physiological dose, typically met in recreational sun exposure during a sunny holiday. FEK4 cells were pre-incubated (or not) with compound **2** and UVA-irradiated.

Figure 3a shows phase contrast microscopy images of the morphological changes occurring following various treatments, 24 h post-irradiation. UVA-irradiated cells exhibited significant swelling that is typical of necrosis (Figure 3a). The morphology of cells treated with compound **2** alone (cpd **2**) or followed by UVA irradiation (cpd **2** + UVA) was indistinguishable from that of untreated control cells (no UVA). When cells were pre-treated with a complex of compound **2** saturated with iron prior to irradiation, the damage incurred appeared similar to that observed with UVA alone. Taken together, these results demonstrate that the mitochondria-targeted compound **2** is capable of protecting the cells against UVA-induced damage. This unprecedented level of protection appears to be due to the strong iron-scavenging activity of compound **2,** since it is abrogated upon complexation of compound **2** with iron (cpd **2**-Fe).

We also scored the percentages of live, apoptotic and necrotic cells by flow cytometry using dual staining with Annexin V-FLUOS/propidium iodide (PI) 24 h after UVA treatment (see Supplementary Information). Representative Annexin V versus PI scatter plots are shown in Figure 3b and the percentages of live cells are plotted in Figure 3c. Untreated control, cpd **2**-treated and cpd **2**-Fe–treated cells all exhibited similar high levels of live populations (*ca* 90%, Figure 3b). UVA induced predominantly necrotic cell death (*ca* 40%, Figure 3b), consistent with the morphologic changes observed microscopically. Furthermore, the percentage of cells undergoing apoptosis in UVA-irradiated samples remained low (*ca* 14%, Figure 3b). 50 μM compound **2** afforded full protection against UVA-induced cell death as seen by restoration of

percentage of live cells to control levels (Figures 3b and 3c). Photoprotection was concentration-dependent and could be observed with as low as 5 μM compound **2** (Figure S4). Compound **4**, a form of compound **2** less able to bind iron, afforded half of the protection provided by the latter, while compound **1** (with no iron-binding activity) had no effect on cell survival when incubated with cells prior to UVA irradiation (Figure 3c). Finally, in line with the morphological observations made in Figure 3a, pre-treatment of cells with the "inactive" (iron-complexed) chelator-peptide failed to protect them against UVA-induced necrotic cell death (Figures 3b and 3c). The complex *per se* did not generate any significant toxicity. The protective effects observed with compound **2** were reproducible with the Dns-labeled version compound **3**, indicating that the Dns fluorophore does not alter the biological function of the chelator-peptide, as previously observed (Abbate et al., 2015a). In FCP7 fibroblasts, compound **2** afforded full protection against UVA radiation in an iron-dependent fashion (Figure S5b), confirming the results obtained with FEK4 cells.

The tricatechol peptide prevents the loss of mitochondria membrane potential associated with UVA irradiation

Loss of mitochondrial membrane potential is an early consequence of UVA radiation-mediated oxidative damage to mitochondrial membrane (Zhong et al., 2004; Pourzand and Tyrrell, 1999). Since compound **2** localizes specifically to the mitochondria, we sought to identify if its mechanism of protection involved the prevention of mitochondrial membrane depolarisation. For this purpose, FEK4 cells were pre-incubated (or not) with compound **2** and irradiated with 500 kJ/m^2 UVA. They were then incubated with the mitochondria-specific red fluorescent cationic dye tetramethylrhodamine methyl ester (TMRM) and analysed by flow cytometry 2 h and 24 h after UVA. A decrease in TMRM fluorescence is indicative of mitochondrial membrane depolarisation.

The results (Figures 4a and 4b) revealed that UVA induced a dramatic drop in TMRM fluorescence already at the 2 h time point. This drop was similar to the depolarisation caused by the mitochondrial membrane uncoupling compound FCCP (data not shown). However, pre-treatment with compound **2** provided a significant protection at that time point. While at 24 h time point, there was a partial but noticeable recovery of TMRM fluorescence in cells treated with UVA, full recovery of membrane potential could be observed in compound **2**-treated cells. In contrast, compound **4** was not able to prevent significantly the UVA-induced decrease in mitochondrial membrane potential at 2 h post-irradiation, in line with its lower iron-binding capability. Nevertheless, it afforded an intermediate level of protection at the 24 h time-point, although less marked than that observed with compound **2**. Taken together, these results show a direct link between the UVA-induced mitochondrial membrane damage and necrotic cell death, both of which could be fully prevented by pre-treatment with the mitochondrial iron chelator compound **2.** Similar results were obtained using FCP7 cells (Figure S5c), albeit revealing a higher sensitivity to UVA-induced mitochondrial damage when compared to FEK4 cells.

The protective effect of mitochondria-targeted chelator compound 2 on ATP depletion associated with UVA-mediated necrosis

We investigated if the protection of the mitochondrial membrane potential afforded by compound **2** upon UVA irradiation correlated with a protection against ATP depletion. The measurement of the intracellular level of ATP 4 h (data not shown) and 24 h after UVA irradiation (Figure 4c) showed that UVA irradiation depleted up to 80% of ATP levels compared to unirradiated control cells, as previously observed (Zhong et al., 2004). Pre-treatment of cells with compound **2** significantly recovered the ATP levels to 60% of the control level at both time points (Figure 4c and data not shown). This level of protection against ATP depletion appears to be sufficient to prevent necrotic cell death induced by UVA (Figure 3). Furthermore, the

protection afforded by compound **2** against UVA-induced ATP depletion appeared to be iron-dependent since its complexation with iron abolished its protective effect. In a similar fashion to FEK4 cells, compound **2** diminished UVA-induced ATP depletion (Figure S5d) in FCP7 cells.

DISCUSSION

We have shown that the mitochondria-targeted compound **2** provides an unprecedented protection against oxidative damage and cell death induced by a high but environmentally relevant dose of UVA in primary skin fibroblast cells. The abrogation of cell death by these chelator-peptides is entirely iron-dependent, since their iron saturation abolished their photoprotective effect. Furthermore partial impairment of the iron binding capability of one of the catechol moieties in compound **4**, significantly reduced its photoprotective ability (Figure 3c).

We chose an 'SS-like peptide' for the effective delivery of our hexadentate iron chelator to the organelle, due to the known mitochondrial selectivity of this family of peptides (Zhao et al., 2003; Szeto, 2008; Szeto and Schiller, 2011; Abbate et al., 2015a and b). These peptides as well as some recently described cationic and lipophilic peptides (Horton et al., 2008; Yousif et al., 2009) have been used successfully as carriers of functional molecules (including antioxidants or drugs) to the mitochondria (Zhao et al., 2004; Zhao et al., 2005; Pereira and Kelley, 2011). These aromatic-cationic peptides, unlike Mito Q, are not taken up due to mitochondrial membrane potential ($\Delta\psi_m$) as they are reported to be concentrated in depolarized mitochondria (Doughan and Dikalov, 2007; Cerrato et al., 2015).

It is essential that the iron chelating peptides we describe herein do not interfere with the normal cellular ferrokinetic pathways, otherwise serious toxic side-effects could be anticipated. Hexadentate catechols are highly selective for iron(III), the oxidation state of iron that accumulates in situations of both iron overload and the uncontrolled lysis of lysosomes. Whereas the cytosol contains a labile iron pool of iron(II), the lysosomes possess a high content

of ferritin, which in turn contains iron(III). Although hexadentate catechols can autoxidise iron(II), the rates of this reaction are extremely slow at iron concentrations of 1-2 µM which are typically found in mammalian cell cytosol (Hider and Kong, 2013). Thus we do not anticipate appreciable interference with the cytosolic iron pool or mitochondrial iron pool, which is also dominated by iron(II), under normal physiological conditions (Ma et al., 2015). A similar situation occurs with deferiprone, a hydroxypyridin-4-one, which has been used for over twenty years in clinical practice for the treatment of iron overload. Like hexadentate catechols, deferiprone is highly selective for iron(III). Although it facilitates the autoxidation of iron(II), it does so at an extremely low rate at low µM concentrations (Devanur et al., 2008).

The role of LI in UVA-induced oxidative damage and necrotic cell death has long been established (Morliere et al., 1991; Pourzand and Tyrrell, 1999; Kvam et al., 2000; Dissemond et al., 2003; Zhong et al., 2004). Earlier studies focussed more on oxidant-mediated destabilisation of lysosomes (Pourzand et al., 1999; Yu et al., 2003; Basu-Modak et al., 2006; Fakih et al., 2008). However subsequent studies recognised mitochondria as the principal destination of LI in cells and therefore a primary site of pro-oxidant generation rendering these organelles particularly susceptible to oxidative damage. Indeed high levels of chelatable LI have been detected by several groups in the mitochondria of cultured cells using various probes (Rauen et al., 2007; Glickstein et al., 2005; Petrat et al., 2002). Additional studies by us have established that the oxidant-induced destabilisation of mitochondrial membrane resulting from intra-mitochondrial Fenton reactions is one of the early cellular events occurring after UVA irradiation of skin cells (Zhong et al., 2004; Yiakouvaki et al., 2006). This provokes a loss of mitochondrial membrane potential and ATP depletion leading irreversibly to necrotic cell death (Zou et al., 1999; Green and Reed, 1998) which can be prevented by iron chelators such as salicylaldehyde isonicotinoyl hydrazone (SIH). This is due to the capability of these compounds to not only deplete the cytosolic LIP but also to access and sequester the loosely available LI in both lysosomal and mitochondrial compartments (Yiakouvaki et al., 2006; Pelle et al., 2011; Simunek

et al., 2005). An inevitable consequence of prolonged non-targeted chelating activity of such chelators is unwanted cytotoxicity (Reelfs et al., 2010; Yu et al., 2006). Compound **2**, which is entirely localized to the mitochondria is expected not to display such undesired side effects. Indeed, time-course studies performed in our laboratory comparing compound **2** and SIH show that unlike SIH, compound **2** does not exhibit any cytotoxicity at the highest tested concentration of 100 μM up to 48 h exposure (see Figure S6). Our results in the two cell lines FEK4 and FCP7 clearly show that compound **2** is fully protective against UVA-induced necrotic cell death despite showing a partial protection against ATP depletion. This phenomenon has already been observed in an unrelated study with Jurkat T cells treated with H_2O_2 showing that iron chelators were effective at protecting cells against necrotic cell death yet not being fully effective in protecting against ATP depletion. This suggests that oxidant-induced ATP depletion is only partially iron-dependent. A plausible iron-independent mechanism would involve oxidant-induced damage to mitochondrial respiratory chain proteins. Because both UVA and H_2O_2 are glutathione-depleting agents (Lautier et al., 1992; Al-Qenaie et al., 2014), protein oxidative damage would be exacerbated under these conditions. Further studies are necessary to unravel these iron-independent mechanisms but this is out of the scope of this study. Nevertheless, it appears that following UVA or H_2O_2 treatment, cells may only need to reach a threshold level of ATP production to be able to fully evade necrotic cell death. This is strengthened by the observation that partial replenishment of ATP by glucose supplementation can rescue skin fibroblasts from UVA-induced necrotic cell death (Zhong et al., 2004).

The importance of mitochondrial LI in oxidative injuries has also been demonstrated in a series of genetic disorders with defective cellular iron utilization (i.e. trafficking and incorporation into proteins) resulting in toxic increase in iron concentrations in mitochondria of excitable cells often leaving the cytosol iron-depleted (Kakhlon et al., 2010; Richardson et al., 2010). For example cultured fibroblasts from Friedreich's ataxia (FRDA) patients that contain high mitochondrial iron level have been shown to be highly sensitive to iron stress and significantly more sensitive to

H_2O_2-induced cell death than fibroblasts from healthy individuals (Wong et al., 1999; Lim et al., 2008). The highly specific and mitochondria-targeted iron chelator designed in this study should therefore be beneficial for the therapy of mitochondrial iron-related oxidative injuries and pathological conditions such as FRDA. While recently a series of mitochondria-targeted antioxidants have been proposed for the therapy of mitochondria-related pathologies (Jauslin et al., 2003; Jauslin et al., 2007; Zhao et al., 2004; Zhao et al., 2005), to our knowledge a highly specific mitochondria-targeted iron chelator such as the one introduced here has not yet been reported.

A variety of iron chelator molecules have been patented as part of sunscreen formulations (Reelfs et al., 2010). While their mild iron chelating properties provide protection against UVB-induced damage, studies from this laboratory and others have demonstrated that these compounds are not effective against UVA-induced iron damage (Reelfs et al., 2010; Aroun et al., 2012; Creighton-Gutteridge and Tyrrell, 2002). For efficient protection against UVA-induced iron damage of skin, strong chelators are required. However these are incompatible with prolonged systemic administration due to toxic effects caused by iron starvation of healthy cells. The mitochondria-targeted chelator-peptide compound **2** provides a solution to this problem and thus can address the current unmet need in the skin care/sunscreen field for potent sunscreen ingredients that are targeted specifically to the principal site of the damage (*i.e.* mitochondria) in the skin cells and are highly effective UVA photoprotectant. It can argued that compound **2** may have an effect on iron-sulfur cluster and/or heme synthesis. Although these important issues are out of the scope of this manuscript, we plan to address them in the near future.

In daily life, skin cells are clearly not exposed exclusively to the UVA waveband but to the entire solar spectrum which also includes UVB. We are introducing the strategy of iron chelation as photoprotectant with the intent to incorporate the chelating molecule as an ingredient to a sunscreen formulation designed to protect against both UVA and UVB components of sunlight. Current filters provide ‘passive’ protection by absorbing and reflecting harmful UV rays from the

skin. Manufacturers have adopted an alternative strategy of adding antioxidants such as vitamins C and E, to their sunscreen products which offers 'active' protection by boosting the body's natural antioxidant reserve to quench any ROS generated from UVA that has passed the UV filters. Despite the attractive nature of this photoprotection strategy, numerous studies in this field have demonstrated that 'conventional' antioxidants which scavenge ROS (*e.g.* vitamins C and E,) have only a very modest protective effect (Reelfs et al., 2010). However studies from our laboratory and others have demonstrated that iron, and in particular mitochondrial iron, plays a major role in the oxidative damage caused by UVA (Aroun et al., 2012). Within this context, we propose that our mitochondria-targeted iron chelator be added as an essential UVA photoprotectant to sunscreen formulations.

MATERIALS AND METHODS

Chelator and Peptide Synthesis

See Supplementary Information for protocols and characterization information.

Reagents

For cell cultivation, all reagents used were cell culture-grade and purchased from Life Technologies (Paisley, Scotland), except foetal calf serum (FCS), which was from Life Technologies Ltd (Paisley, UK) and phosphate buffered saline (PBS) from Oxoid Ltd (Basingstoke, UK). TMRM and the organelle-specific markers MitoTracker® Deep Red FM, Lyso Tracker® Deep Red and ER Tracker™ Red were purchased from Invitrogen (Paisley, Scotland). Annexin V-FLUOS was from Roche (Welwyn Garden City, UK). All other reagents were from Sigma-Aldrich (Gillingham, UK).

Cell culture

The human primary fibroblasts FEK4 and FCP7 were a kind gift from Prof. Tyrrell's laboratory and were grown as described previously (Abbate et al., 2015a). The foreskin fibroblast cultures were initiated in Prof. Tyrrell's laboratory, Switzerland, from tissue samples obtained in full compliance with ethical regulations and legislation in force at the time and respecting complete donor confidentiality. Patient consent for experiments was not required because under Swiss laws in force at the time, human material left over from surgery was considered as discarded material. These cells have been isolated from foreskin biopsies at passage 0. From that, sub-cultured and frozen stocks between passage 1 and 12 were available for the present study.

Treatments and peptide delivery

The (chelator)-peptides were prepared as 100 mM stock solutions in DMSO. They were diluted to the desired final concentration (50 μM unless specified) and added to cells overnight as described previously (Abbate et al., 2015a and b).

UVA irradiation

Irradiations were performed in PBS at approximately 25 ℃ using a broad spectrum Sellas 4 kW UVA lamp (Sellas, Germany), as described previously (Pourzand et al., 1999).

Flow cytometry and Live cell microscopy

All flow cytometry- and live cell microscopy-based protocols are described in Supplementary Information file.

ATP measurement

ATP production by cells following various treatments was monitored with a luminometer (Turner Designs Model TD-20/20) 24 h after UVA, using the ViaLight™ plus kit (Lonza Biologics plc, Slough, U.K.) as described previously (Al-Qenaei et al., 2014).

Iron complexation

Iron:ligand complexes were prepared by mixing equimolar amounts of iron(III) as $FeCl_3 \bullet 6H_2O$ and the hexadentate-peptide molecule. The complex was allowed to form for 1 h at room temperature prior to incubation with the cells overnight at 37 ℃ at a final concentration of 50 μM.

Statistical methods

Results are expressed as the mean +/- SD. Significant differences ($P < 0.05$) were determined by either paired or unpaired t-test after one-way analysis of variance.

CONFLICT OF INTEREST

The authors state no conflict of interest.

ACKNOWLEDGMENTS

We are grateful to Prof. Rex Tyrrell for the gift of the cell lines and for useful discussion. We also thank Prof. David Tosh for letting us use his epifluorescence microscope and Dr Adrian Rogers for his support with the flow cytometry. This work was funded by Biotechnology and Biological Sciences Research Council (BBSRC, Grant no BB/J005223/1).

REFERENCES

Abbate V, Reelfs O, Hider RC, Pourzand C. Design of novel fluorescent mitochondria targeted peptides with iron-selective sensing activity. Biochem J 2015a;469:357-66.

Abbate V, Reelfs O, Kong X, Pourzand C, Hider RC. Dual selective iron chelating probes with a potential to monitor mitochondrial labile iron pools. Chem Commun (Camb) 2015b;2:784-787.

Al-Qenaei A, Yiakouvaki A, Reelfs O, Santambrogio P, Levi S, Hall ND, et al. Role of intracellular labile iron, ferritin, and antioxidant defence in resistance of chronically adapted Jurkat T cells to hydrogen peroxide. Free Radic Biol Med 2014;68:87-100.

Aroun A, Zhong JL, Tyrrell RM, Pourzand C. Iron, oxidative stress and the example of solar ultraviolet A radiation. Photochem Photobiol Sci 2012;11:118-34.

Basu-Modak S, Ali D, Gordon M, Polte T, Yiakouvaki A, Pourzand C, et al. Suppression of UVA-mediated release of labile iron by epicathecin-A link to lysosomal protection. Free Radic Biol Med 2006;41:1197-204.

Berneburg M, Grether-Beck S, Kürten V, Ruzicka T, Briviba K, Sies H, et al. Singlet oxygen mediates the UVA induced generation of the photoaging-associated mitochondrial common deletion. J Biol Chem 1999;274:15345–9.

Cabantchik ZI. Labile iron in cells and body fluids: physiology, pathology, and pharmacology. Front Pharmacol 2014;5:45.

Cerrato CP, Pirisinu M, Vlachos EN, Langel Ü. Novel cell-penetrating peptide targeting mitochondria. FASEB J 2015;29:4589-99.

Creighton-Gutteridge M, Tyrrell RM. A novel iron chelator that does not induce HIF-1 activity. Free Radic Biol Med 2002;33:356-63.

Devanur LD, Neubert H, Hider RC. The fenton activity of iron(III) in the presence of deferiprone. J Pharm Sci 2008;97:1454-67.

Dissemond J, Schneider LA, Brenneisen P, Briviba K, Wenk J, Wlaschek M, et al. Protective and determining factors for the overall lipid peroxidation in ultraviolet A1-irradiated fibroblasts: *in vitro* and *in vivo* investigations. Br J Dermatol 2003;149:341-9.

Doughan AK, Dikalov SI. Mitochondrial redox cycling of mitoquinone leads to superoxide production and cellular apoptosis. Antioxid Redox Signal 2007;9:1825-36.

Fakih S, Podinovskaia M, Kong X, Collins HL, Schaible UE, Hider RC. Targeting the lysosome: fluorescent iron(III) chelators to selectively monitor endosomal/lysosomal labile iron pools. J Med Chem 2008;51:4539-52.

Glickstein H, El RB, Shvartsman M, Cabantchik ZI. Intracellular labile iron pools as direct targets of iron chelators: a fluorescence study of chelator action in living cells. Blood 2005;106:3242-50.

Green DR, Reed JC. Mitochondria and apoptosis. Science 1998;281:1309-12.

Hider RC, Kong X. Iron speciation in the cytosol: an overview. Dalton Trans 2013;42:3220-9.

Hider RC, Zhou T. The design of orally active iron chelators. Ann N Y Acad Sci 2005;1054:141-54.

Horton KL, Stewart KM, Fonseca SB, Guo Q, Kelley SO. Mitochondria-penetrating peptides. Chem Biol 2008;15:375-82.

James AM, Harpley MS, Manas AR, Frerman FE, Hirst J, Smith RA, et al. Interaction of the mitochondria targeted antioxidant MitoQ with phospholipid bilayers and ubiquinone oxidoreductases. J Biol Chem 2007;282**:**14708–18.

Jauslin ML, Meier T, Smith RA, Murphy MP. Mitochondria-targeted antioxidants protect Friedreich Ataxia fibroblasts from endogenous oxidative stress more effectively than untargeted antioxidants. FASEB J 2003;17:1972-4.

Jauslin ML, Vertuani S, Durini E, Buzzoni L, Ciliberti N, Verdecchia S, et al. Protective effects of Fe-Aox29, a novel antioxidant derived from a molecular combination of Idebenone and vitamin E, in immortalized fibroblasts and fibroblasts from patients with Friedreich Ataxia. Mol Cell Biochem 2007;302:79-85.

Kakhlon O, Breuer W, Munnich A, Cabantchik ZI. Iron redistribution as a therapeutic strategy for treating diseases of localized iron accumulation. Can J Physiol Pharmacol 2010;88:187-96.

Krishna CM, Liebmann JE, Kaufman D, DeGraff W, Hahn SM, McMurry T, et al. The catecholic metal sequestering agent 1,2-dihydroxybenzene-3,5-disulfonate confers protection against oxidative cell damage. Arch Biochem Biophys 1992;294**:**98–106.

Krishnan KJ, Birch-Machin MA. The incidence of both tandem duplications and the common deletion in mtDNA from three distinct categories of sun-exposed human skin and in prolonged culture of fibroblasts. J Invest Dermatol 2005;126:408–15.

Kvam E, Hejmadi V, Ryter S, Pourzand C, Tyrrell RM. Heme oxygenase activity causes transient hypersensitivity to oxidative ultraviolet A radiation that depends on release of iron from heme. Free Radic Biol Med 2000;28:1191-6.

Lautier D, Luscher P, Tyrrell RM. Endogenous glutathione levels modulate both constitutive and UVA radiation/hydrogen peroxide inducible expression of the human heme oxygenase gene. Carcinogenesis 1992;13:227-32.

Leist M, Single B, Castoldi AF, Kühnle S, Nicotera P. Intracellular adenosine triphosphate (ATP) concentration: a switch in the decision between apoptosis and necrosis. J Exp Med 1997;185:1481-6.

Levi S, Rovida E. The role of iron in mitochondrial function. Biochim Biophys Acta 2009;1790:629-36.

Li P, Nijhawan D, Budihardjo I, Srinivasula SM, Ahmad M, Alnemri ES, et al. Cytochrome c and dATP-dependent formation of Apaf-1/caspase-9 complex initiates an apoptotic protease cascade. Cell 1997;91:479-89.

Lim CK, Kalinowski DS, Richardson DR. Protection against hydrogen peroxide-mediated cytotoxicity in Friedreich's ataxia fibroblasts using novel iron chelators of the 2 pyridylcarboxaldehyde isonicotinoyl hydrazone class. Mol Pharmacol 2008;74:225-35.

Liu ZD, Hider RC. Design of iron chelators with therapeutic application. Coord Chem Rev 2002;232:151–71.

Ma Y, Abbate V, Hider RC. Iron-sensitive fluorescent probes: monitoring intracellular iron pools. Metallomics 2015;7:212-22.

McArdle F, Pattwell DM, Vasilaki A, McArdle A, Jackson MJ. Intracellular generation of reactive oxygen species by contracting skeletal muscle cells. Free Radic Biol Med 2005;39:651–57.

Morlière P, Moysan A, Santus R, Hüppe G, Mazière JC, Dubertret L. UVA-induced lipid peroxidation in cultured human fibroblasts. Biochim Biophys Acta 1991;1084:261-268.

Murphy MP. How mitochondria produce reactive oxygen species. Biochem J 2009;417:1-13.

Oyewole AO, Wilmot M-C, Fowler M, Birch-Machin MA. Comparing the effects of mitochondrial targeted and localized antioxidants with cellular antioxidants in human skin cells exposed to UVA and hydrogen peroxide. FASEB J 2014;28:485–94.

Paradkar PN, Zumbrennen KB, Paw BH, Ward DM, Kaplan J. Regulation of mitochondrial iron import through differential turnover of mitoferrin 1 and mitoferrin 2. Mol Cell Biol 2009;29:1007-16.

Pelle E, Jian J, Declercq L, Dong K, Yang Q, Pourzand C, et al. Protection against ultraviolet A –induced oxidative damage in normal human epidermal keratinocytes under post-menopausal conditions by an ultraviolet A-activated caged-iron chelator: a pilot study. Photodermatol Photoimmunol Photomed 2011;27:231-5.

Pereira MP, Kelley SO. Maximizing the therapeutic window of an antimicrobial drug by imparting mitochondrial sequestration in human cells. J Am Chem Soc 2011;133:3260-3.

Petrat F, de Groot H, Rauen U. Subcellular distribution of chelatable iron: a laser scanning microscopic study in isolated hepatocytes and liver endothelial cells. Biochem J 2001;356:61-9.

Petrat F, Weisheit D, Lensen M, de Groot H, Sustmann R, Rauen U. Selective determination of mitochondrial chelatable iron in viable cells with a new fluorescent sensor. Biochem J 2002;362:137-47.

Pourzand C, Watkin RD, Brown JE, Tyrrell RM. Ultraviolet A radiation induces immediate release of iron in human primary skin fibroblasts: the role of ferritin. Proc Natl Acad Sci U S A 1999;96:6751-6.

Pourzand C, Tyrrell RM. Apoptosis, the role of oxidative stress and the example of solar UV radiation. Photochem Photobiol 1999;70:380-90.

Rauen U, Springer A, Weisheit D, Petrat F, Korth HG, de Groot H, et al. Assessment of chelatable mitochondrial iron by using mitochondrion-selective fluorescent iron indicators with different iron-binding affinities. Chembiochem 2007;8:341-52.

Reelfs O, Eggleston IM, Pourzand C. Skin protection against UVA-induced iron damage by multiantioxidants and iron chelating drugs/prodrugs. Curr Drug Metab 2010;11:242-49.

Reelfs O, Tyrrell RM, Pourzand C. Ultraviolet a radiation-induced immediate iron release is a key modulator of the activation of NF-kappaB in human skin fibroblasts. J Invest Dermatol 2004;122:1440-7.

Richardson DR, Huang ML, Whitnall M, Becker EM, Ponka P, Suryo Rahmanto Y. The ins and outs of mitochondrial iron-loading: the metabolic defect in Friedreich's ataxia. J Mol Med (Berl) 2010;88:323-9.

Simunek T, Boer C, Bouwman RA, Vlasblom R, Versteilen AM, Sterba M, et al. SIH, a novel lipophilic iron chelator, protects H9c2 cardiomyoblasts from oxidative stress-induced mitochondrial injury and cell death. J Mol Cell Cardiol 2005;39:345-54.

Shaw GC, Cope JJ, Li L Corson K, Hersey C, Ackermann GE, et al. Mitoferrin is essential for erythroid iron assimilation. Nature 2006;440:96-100.

Shidoji Y, Hayashi K, Komura S, Ohishi N, Yagi K. Loss of molecular interaction between cytochrome c and cardiolipin due to lipid peroxidation. Biochem Biophys Res Commun 1999;264:343-7.

Sohn YS, Breuer W, Munnich A, Cabantchik ZI. Redistribution of accumulated cell iron: a modality of chelation with therapeutic implications. Blood 2008;111(3):1690-9.

Szeto HH. Development of mitochondria-targeted aromatic-cationic peptides for neurodegenerative diseases. Ann N Y Acad Sci 2008;1147:112-21.

Szeto HH, Schiller PW. Novel therapies targeting inner mitochondrial membrane--from discovery to clinical development. Pharm Res 2011;28:2669-79.

Tulah AS, Birch-Machin MA. Stressed out mitochondria: the role of mitochondria in ageing and cancer focussing on strategies and opportunities in human skin. Mitochondrion 2013;13**:**444–53.

Tyrrell RM. Activation of mammalian gene expression by the UV component of sunlight-from models to reality. BioEssays 1996;18:139-48.

Winterbourn CC. Reconciling the chemistry and biology of reactive oxygen species. Nat Chem Biol 2008;4:278-86.

Wong A, Yang J, Cavadini P, Gellera C, Lonnerdal B, Taroni F, et al. The Friedreich's ataxia mutation confers cellular sensitivity to oxidant stress which is rescued by chelators of iron and calcium and inhibitors of apoptosis. Hum Mol Genet 1999;8:425-30.

Yiakouvaki A, Savović J, Al-Qenaei A, Dowden J, Pourzand C. Caged-iron chelators a novel approach towards protecting skin cells against UVA-induced necrotic cell death. J Invest Dermatol 2006;126:2287-95.

Yousif LF, Stewart KM, Horton KL, Kelley SO. Mitochondria-penetrating peptides: sequence effects and model cargo transport. Chembiochem 2009;10:2081-8.

Yu Y, Wong J, Lovejoy DB, Kalinowski DS, Richardson DR. Chelators at the cancer coalface: desferrioxamine to Triapine and beyond. Clin Cancer Res 2006;12:6876-83.

Yu Z, Persson HL, Eaton JW, Brunk UT. Intralysosomal iron: a major determinant of oxidant-induced cell death. Free Radic Biol Med 2003;34:1243-52.

Zhao K, Luo G, Giannelli S, Szeto HH. Mitochondria-targeted peptide prevents mitochondrial depolarization and apoptosis induced by tert-butyl hydroperoxide in neuronal cell lines. Biochem Pharmacol 2005;70:1796-806.

Zhao K, Luo G, Zhao GM, Schiller PW, Szeto HH. Transcellular transport of a highly polar 3+ net charge opioid tetrapeptide. J Pharmacol Exp Ther 2003;304:425-32.

Zhao K, Zhao GM, Wu D, Soong Y, Birk AV, Schiller PW, et al. Cell-permeable peptide antioxidants targeted to inner mitochondrial membrane inhibit mitochondrial swelling, oxidative cell death, and reperfusion injury. J Biol Chem 2004;279:34682-90.

Zhong JL, Yiakouvaki A, Holley P, Tyrrell RM, Pourzand C. Susceptibility of skin cells to UVA-induced necrotic cell death reflects the intracellular level of labile iron. J Invest Dermatol 2004;123:771-80.

Zou H, Li Y, Liu X, Wang X. An APAF-1.cytochrome c multimeric complex is a functional apoptosome that activates procaspase-9. J Biol Chem 1999;274:11549-56.

FIGURE LEGENDS

Figure 1: Structures of compounds 1-4.

The structures of the compounds investigated are depicted with their ionized functions at pH 7.4. Iron-binding functions are indicated in blue. The dansyl (Dns) fluorophore is indicated in red.

Figure 2. Microscopy images of subcellular localization studies of the DNS-labelled peptide-chelator H-Hbl-Hbl-Hbl-r-F-DAP(Dns)-NH_2 (compound 3).

Representative microscopy images are shown, of cells stained with compound **3** in combination with markers for mitochondrial (**a-d**), lysosomal (**e-h**) and ER (**i-l**) compartments. Fluorescence data were collected and analysed as described in Materials and Methods. Green (**b, f, j**) and red (**c, g, k**) fluorescence data were merged together (**d, h, l**) to identify co-localization in yellow. The phase contrast images (**a, e, i**) corresponding to the fluorescence data are also shown. Scale bar = 10 μm.

Figure 3. Compound 2 protects FEK4 cells from UVA-induced cell death.

Cells were treated with compound **2** (cpd **2**) alone or as a complex with iron (cpd **2**-Fe) or UVA or combinations thereof. **a.** Bright-field images were captured 24 h post-treatment. Swelling (arrows in insert) is indicative of cell death by necrosis and is visible following UVA treatment alone or in combination with cpd **2**-Fe. Scale bar = 50 μm. **b.** Cells treated as described above were processed for flow cytometry analysis as described in Materials and Methods. Dot plots of a representative experiment are shown. Live cells are defined as Annexin V-negative/PI-negative (lower left-hand quadrant). **c.** Bar chart of flow cytometry results, expressed as means

+/- SD of percentage live cells from 3-5 experiments. * Significantly different (p<0.05) from UVA alone. † Significantly different (p<0.05) from cpd **2**+UVA.

Figure 4. Compound 2 significantly reduces UVA-induced damage to mitochondria membrane.

a. Representative fluorescence intensity profiles of samples stained with TMRM at 2 h and 24 h post-UVA irradiation as described in Materials and Methods. **b.** Bar chart of the results of TMRM staining experiments. Fluorescence median intensities (MFIs) collected over the region delineated in panel **a** as P2 are expressed as percentage of untreated control. * Significantly different (p<0.05) from corresponding UVA-treated sample. † Significantly different (p<0.05) from corresponding cpd **2**+UVA-treated sample. **c.** FEK4 cells were pre-treated with either compound **2** alone or as a complex with iron, prior to UVA irradiation and ATP production was measured as described in Materials and Methods. Results are expressed as percentage of untreated control. * Significantly different (p<0.05) from UVA alone sample.

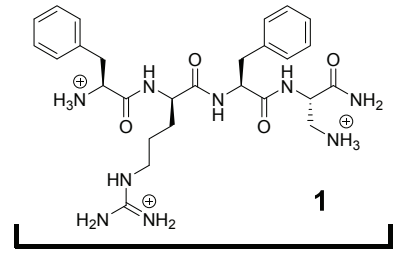

1

Mitochondria-targeted peptide

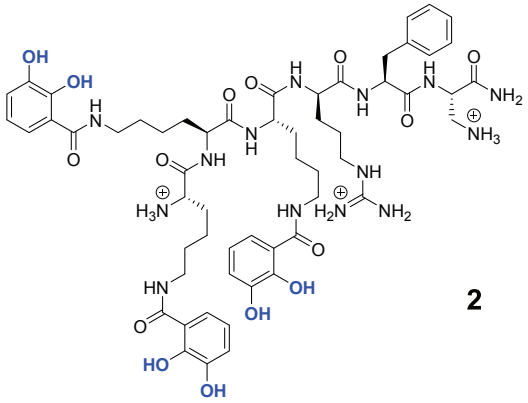

2

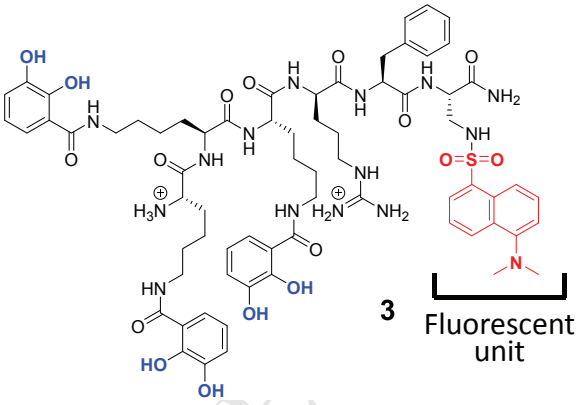

3

Fluorescent unit

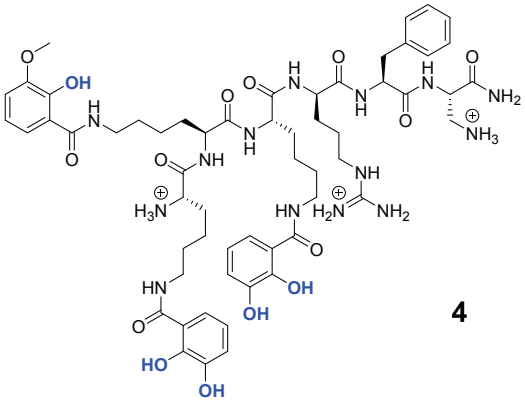

4

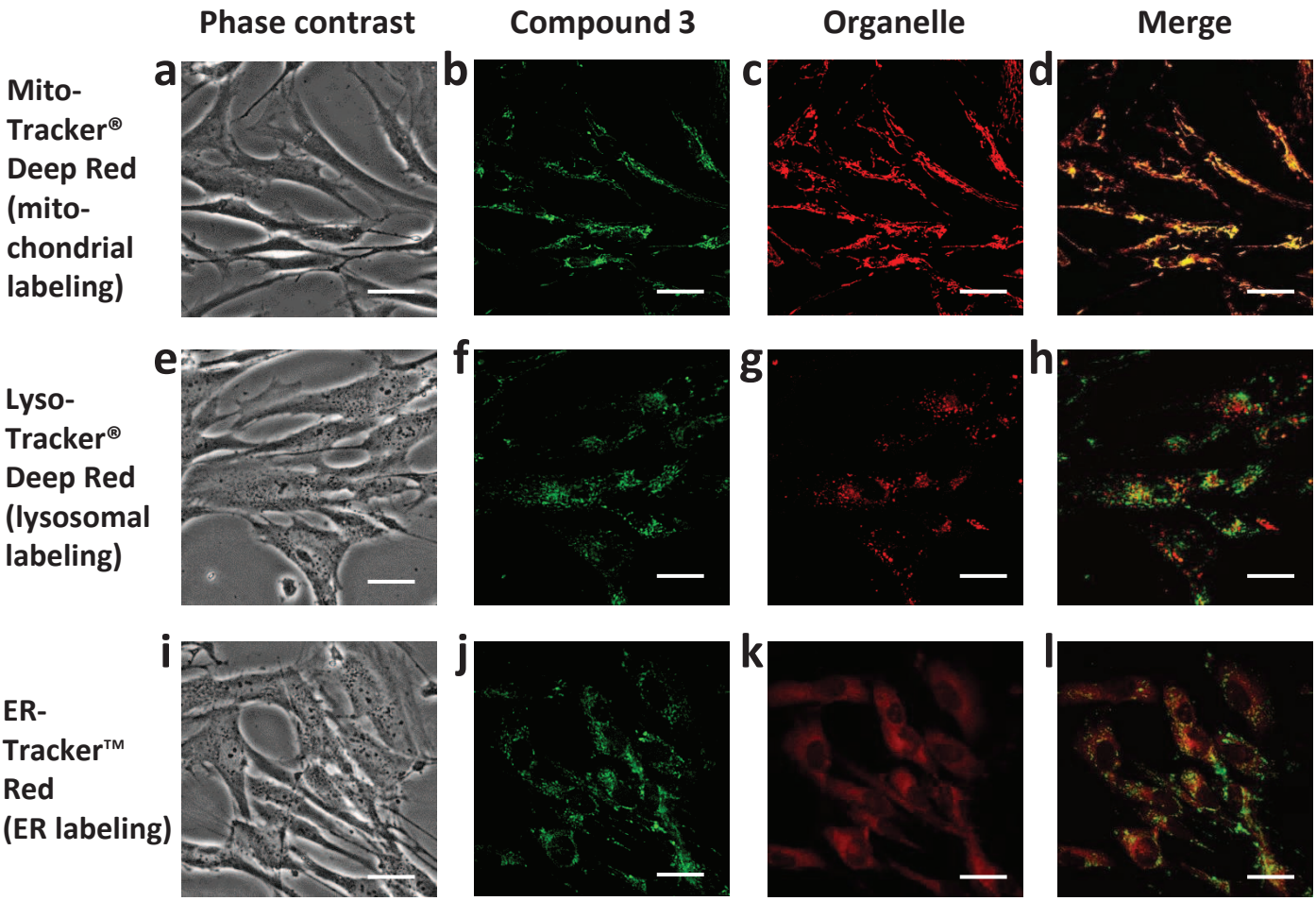
Phase contrast
Compound 3
Organelle
Merge
a
b
c
d
Mito-Tracker® Deep Red (mito-chondrial labeling)
e
f
g
h
Lyso-Tracker® Deep Red (lysosomal labeling)
i
j
k
l
ER-Tracker™ Red (ER labeling)

Figure 2

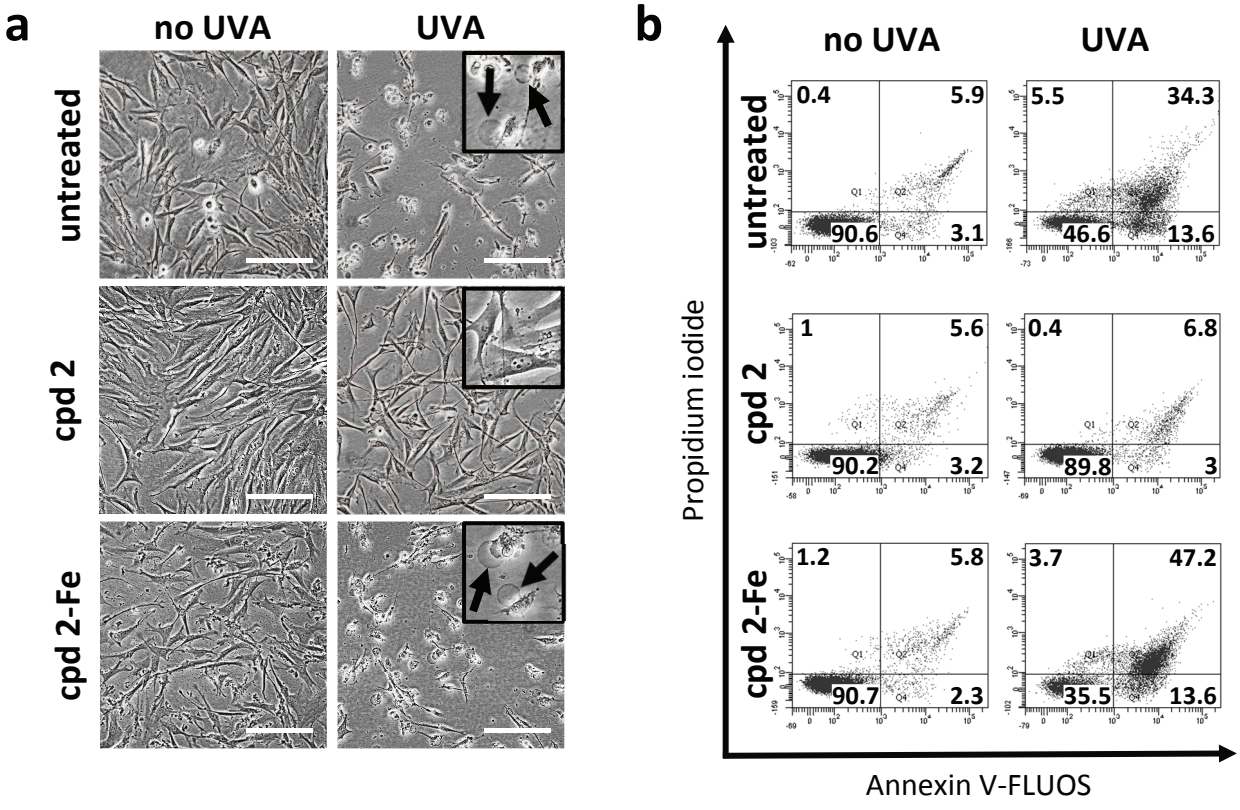
a
no UVA
UVA
untreated
cpd 2
cpd 2-Fe
b
no UVA
UVA
untreated
cpd 2
cpd 2-Fe
0.4
5.9
90.6
3.1
5.5
34.3
46.6
13.6
1
5.6
90.2
3.2
0.4
6.8
89.8
3
1.2
5.8
90.7
2.3
3.7
47.2
35.5
13.6
Propidium iodide
Annexin V-FLUOS

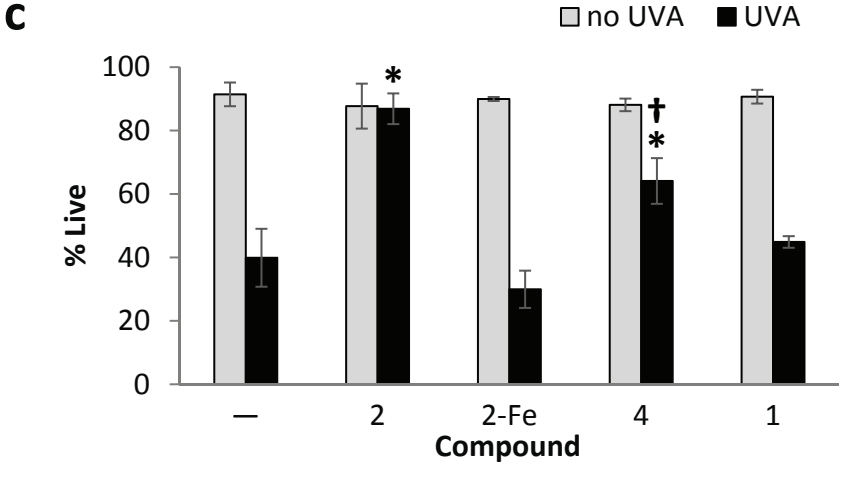
c
no UVA
UVA
100
80
60
40
20
0
% Live
*
*
†
—
2
2-Fe
4
1
Compound

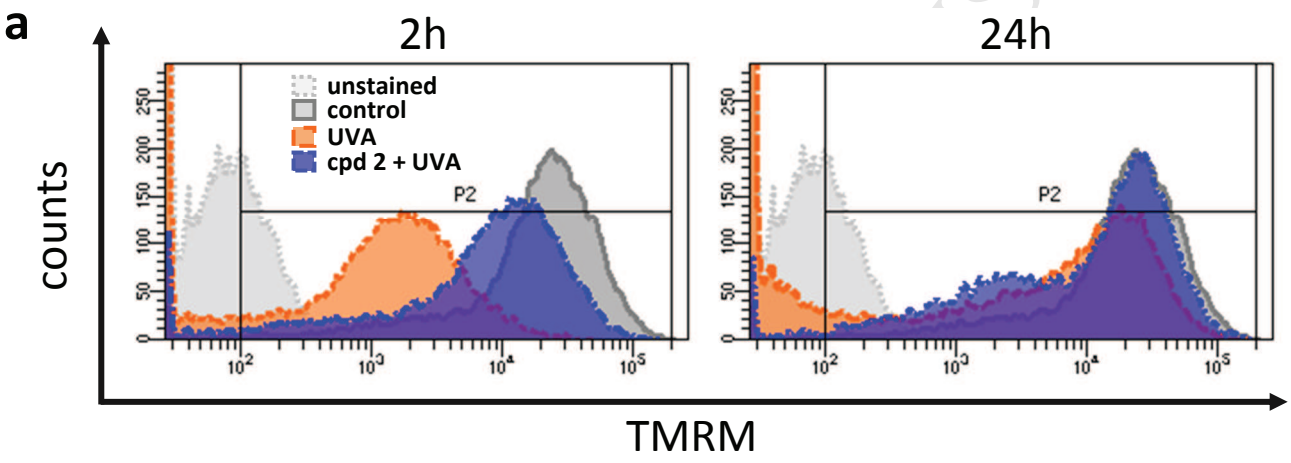
a
2h
24h
unstained
control
UVA
cpd 2 + UVA
P2
P2
counts
TMRM

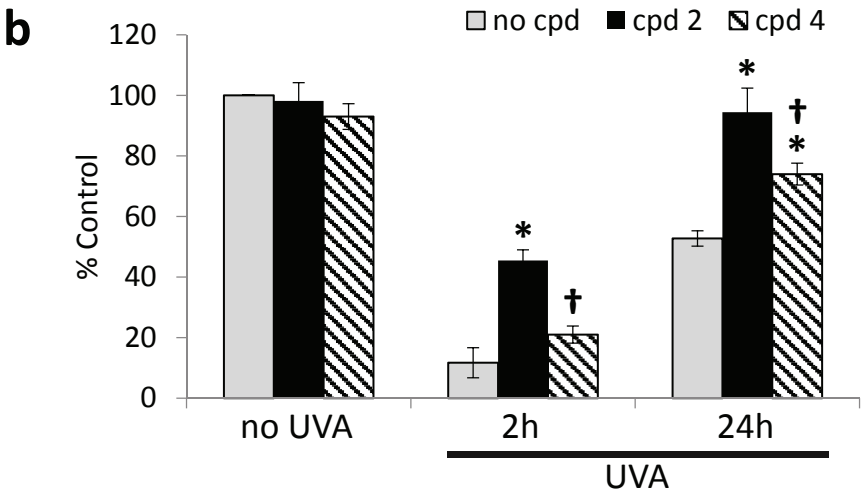
b
no cpd
cpd 2
cpd 4
% Control
no UVA
2h
24h
UVA

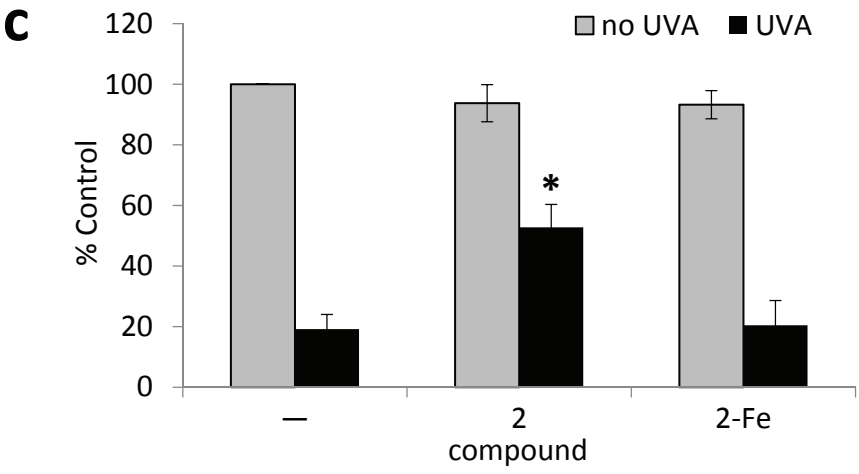
c
no UVA
UVA
% Control
—
2
2-Fe
compound